Title

D-cis-Diltiazem Can Produce Oxidative Stress in Healthy Depolarized Rods In Vivo

Permalink

https://escholarship.org/uc/item/5k7966nh

Journal

Investigative Ophthalmology & Visual Science, 59(7)

ISSN

0146-0404

Authors

Berkowitz, Bruce A
Podolsky, Robert H
Farrell, Benjamin
et al.

Publication Date

2018-06-11

DOI

10.1167/iovs.18-23829

Peer reviewed

D-*cis*-Diltiazem Can Produce Oxidative Stress in Healthy Depolarized Rods In Vivo

Bruce A. Berkowitz,[1,2] Robert H. Podolsky,[3] Benjamin Farrell,[1] Hojun Lee,[1] Christopher Trepanier,[1] Ali M. Berri,[1] Kristin Dernay,[1] Emma Graffice,[1] Fatema Shafie-Khorassani,[3] Timothy S. Kern,[4] and Robin Roberts[1]

[1]Department of Anatomy and Cell Biology, Wayne State University School of Medicine, Detroit, Michigan, United States
[2]Department of Ophthalmology, Wayne State University School of Medicine, Detroit, Michigan, United States
[3]Department of Family Medicine and Public Health Sciences, Wayne State University, Detroit, Michigan, United States
[4]Department of Pharmacology, School of Medicine, Case Western Reserve University, Cleveland, Ohio, United States

PURPOSE. New perspectives are needed to understand decades of contradictory reports on the neuroprotective effects of the Cav1.2 L-type calcium channel blocker d-*cis*-diltiazem in retinitis pigmentosa (RP) models. Here, we address, in vivo, the following two knowledge gaps regarding d-*cis*-diltiazem's actions in the murine outer retina: (1) do normal mouse rods contain d-*cis*-diltiazem-insensitive Cav1.2 L-type calcium channels? (2) Can d-*cis*-diltiazem modify the normal rod redox environment?

METHODS. First, transretinal Cav1.2 L-type calcium channels were noninvasively mapped with manganese-enhanced magnetic resonance imaging (MRI) following agonist Bay K 8644 in C57BL/6 (B6) and in Cav1.2 L-type calcium channel BAY K 8644–insensitive mutant B6 mice. Second, d-*cis*-diltiazem–treated oxidative stress–vulnerable (B6) or –resistant [129S6 (S6)] mice were examined in vivo (QUEnch-assiSTed [QUEST] MRI) and in whole retina ex vivo (lucigenin). Retinal thickness was measured using MRI.

RESULTS. The following results were observed: (1) manganese uptake patterns in BAY K 8644–treated controls and mutant mice identified in vivo Cav1.2 L-type calcium channels in inner and outer retina; and (2) d-*cis*-diltiazem induced rod oxidative stress in dark-adapted B6 mice but not in light-adapted B6 mice or dark-adapted S6 mice (QUEST MRI). Oxidative stress in vivo was limited to inferior outer retina in dark-adapted B6 mice approximately 1-hour post d-*cis*-diltiazem. By approximately 4 hours post, only superior outer retina oxidative stress was observed and whole retinal superoxide production was supernormal. All groups had unremarkable retinal thicknesses.

CONCLUSIONS. D-*cis*-diltiazem's unexpectedly complex spatiotemporal outer retinal oxidative stress pattern in vivo was dependent on genetic background and rod membrane depolarization, but not apparently dependent on Cav1.2 L-type calcium channels, providing a potential rationale for contradictory results in different RP models.

Keywords: MRI, photoreceptors, L-type calcium channels, vision, retinitis pigmentosa

D-*cis*-diltiazem is commonly used clinically because of its useful cardio-protective properties. D-*cis*-diltiazem is usually thought of as an effective blocker of the Cav1.2 L-type calcium channel subtype (IC50s of $\sim$45 µM for $Ca_v1.2$ L-type calcium channels, $\sim$326 µM for $Ca_v1.3$ L-type calcium channels, and $\sim$92 µM for $Ca_v1.4$ L-type calcium channels[1–5]).[6] In 1999, d-*cis*-diltiazem was suggested to have neuroprotective properties in a mouse model of retinitis pigmentosa (RP).[7] However, subsequent research produced contradictory results that either supported,[8–15] or did not support,[16–21] d-*cis*-diltiazem's ability to modify the course of rod degeneration. Most studies focused on d-*cis*-diltiazem's modification of disrupted calcium regulation in RP, and little attention was given to potential cross-linked factors, such as oxidative stress that can also trigger rod atrophy and contribute to RP morbidity.[8–15,22] Here, we step back from examining d-*cis*-diltiazem ex vivo and in the context of RP to examine instead its impact in healthy rod photoreceptor cells in vivo. Our rationale is that a noninvasive

understanding of d-*cis*-diltiazem's actions in the absence of disease might provide new insights into d-*cis*-diltiazem's debatable outcomes in RP.

In the retina, Cav1.2 L-type calcium channels have been localized to the inner retina as measured by immunohistochemistry and also in vivo by d-*cis*-diltiazem–induced inhibition of the uptake of the L-type calcium channel probe manganese in 2- to 5-month C57BL/6 (B6) mice.[1–5] Also, photoreceptors in the outer retina are responsive to d-*cis*-diltiazem, with the synaptic photoreceptor L-type voltage-gated Ca2+ channels identified as a target for d-*cis*-diltiazem based on ex vivo studies involving bovine, salamander, and porcine photoreceptors, or in mice that have retinas that degenerate.[7,10,16,23,24] Yet, there has been uncertainty about these Cav1.2 L-type calcium channels in vivo in healthy murine outer retina, perhaps in part because rod Cav1.2 L-type calcium channels may be unconventional.[3,4,10,23,25] In this study, we take advantage of magnetic resonance imaging's (MRI) robust ability to measure,
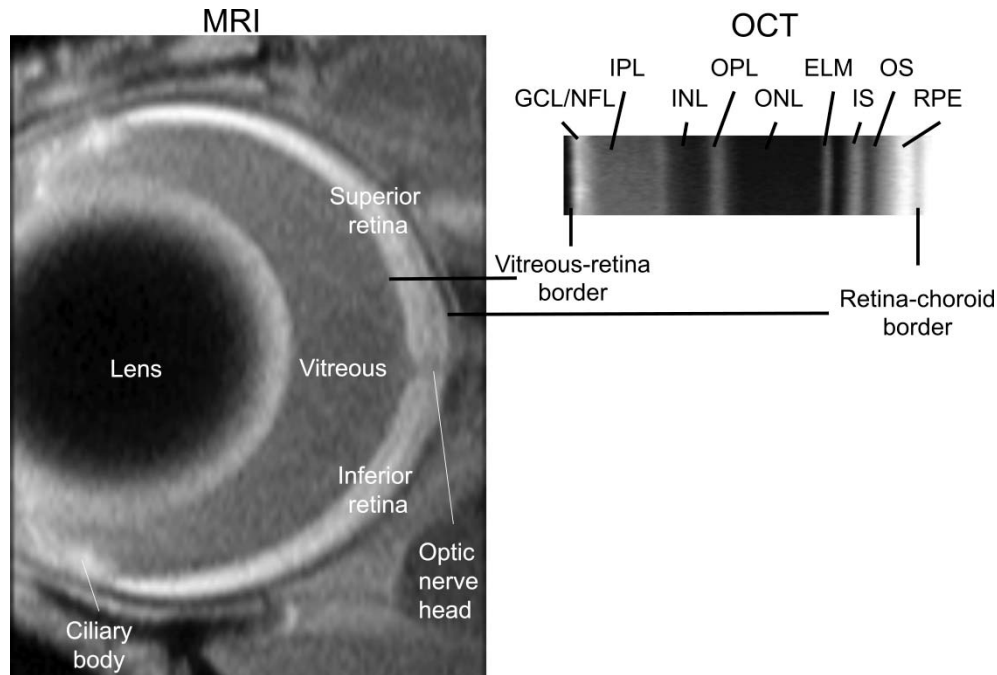
FIGURE 1. Comparison of representative high spatial resolution T1-weighted MRI (*left*) and OCT (*right*) images. The retina shows a distinctive four-layer pattern (bright, dark, bright, dark) on MRI, as previously reported; the anatomic identity of each dark/bright band has not been fully characterized.[110] The vitreous–retina and retina–choroid borders are well defined on both MRI and OCT, and thus these borders are used as the only fiduciary alignment regions for comparing MRI and OCT data in Figures 2 through 7; for clarity, the two borders are shown off-set from each other in the Figure. OCT layer assignments (GCL, ganglion cell layer; INL, inner nuclear layer; IPL, inner plexiform layer; IS, rod inner segment layer; OLM, outer limiting membrane; ONL, outer nuclear layer; OPL, outer plexiform layer; OS, rod outer segment layer) are as previously published.[111]

noninvasively and without depth limitation, transretinal, and more specifically, rod cell subcompartment, uptake of manganese in vivo using manganese-enhanced MRI (MEMRI).[26] MEMRI has been established since 2006 as the imaging modality of choice for studying retinal L-type calcium channel regulation in vivo.[26,27] MEMRI can directly address the above knowledge gap by following treatment in vivo with the dihydropyridine agonist BAY K 8644 K 8644 in B6 and mutant Cav1.2 L-type calcium channel dihydropyridine-insensitive B6 (Cav1.2dihydropyridine$^{-/-}$) mice.[28,29]

Oxidative stress is a pathogenic factor underlying photoreceptor degeneration in RP.[30–34] Intriguingly, the redox environment can be modified by d-*cis*-diltiazem in nonretinal cell types.[35–40] For example, in isolated hepatocytes and in intact liver, d-*cis*-diltiazem has shown antioxidant properties, whereas in testes and sperm cells, d-*cis*-diltiazem promotes excessive production of reactive oxygen species.[35–40] It is not known if d-*cis*-diltiazem alters the redox status of the outer retina in vivo, but if so, this could be an important confounder not previously considered.

In this study, we take advantage of a MRI method that uniquely measures a snapshot of outer retinal excessive production of reactive oxygen species with high-spatial resolution in vivo.[41–43] This approach takes advantage of the fact that free radicals are inherently paramagnetic so that excessive production of reactive oxygen species generates a paramagnetic contrast mechanism detectable on MRI by comparing 1/T1 with and without an antioxidant in different layers of the retina (QUEnch-assiSTed [QUEST] MRI).[41–44] QUEST MRI has been validated as a powerful, noninvasive, and graded measurement of excessive production of reactive oxygen species that does not involve injection of a contrast agent.[41–44] Here, healthy mice were studied at different times after d-*cis*-diltiazem treatment and the administration of either saline or a drug combination that reduces excessive produc-

tion of reactive oxygen species (methylene blue [MB] and α-lipoic acid [ALA]). MB and ALA are two Food and Drug Administration (FDA)-approved drugs with antioxidant properties that are useful for the QUEST MRI examination.[42–44] In subgroups, gold-standard lucigenin superoxide measurements of whole retina were also performed. In addition, we assessed d-*cis*-diltiazem's impact on retinal thicknesses in vivo.

MATERIALS AND METHODS

All mice were treated in accordance with the National Institutes of Health Guide for the Care and Use of Laboratory Animals, the ARVO Statement for the Use of Animals in Ophthalmic and Vision Research, and Institutional Animal and Care Use Committee (IACUC) authorization. Mice were housed and maintained in either full dark conditions, in 12:12-hour light-dark cycle laboratory lighting, or as described below. Mice were humanely euthanized by cervical dislocation followed by a bilateral pneumothorax, as detailed in our IACUC-approved protocol.

Optical coherence tomography (OCT) does not measure rod cell subcompartment L-type calcium channel function or excessive production of free radicals. Instead, we used MRI because its spatial resolution has been validated as sufficient to measure localized functional indices in different retinal layers.[26,41–43]

Groups

The first knowledge gap was tested in the following two groups: (1) 2- to 3-month male C57BL/6 + BAY K 8644 (B6; Jackson Labs, Bar Harbor, ME, USA), and (2) 2- to 3-month male Cav1.2dihydropyridine$^{-/-}$ mice + BAY K 8644 (on a B6 background; a kind gift of breeders by Jörg Striessnig, PhD)
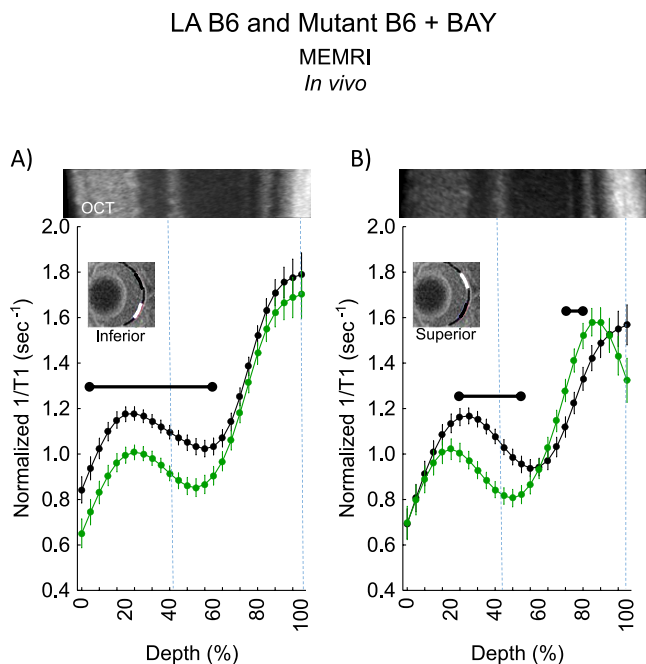
FIGURE 2. Cav1.2 L-type calcium channel retinal topography in light-adapted (LA) B6 mice as measured by MEMRI. Summary of modeling results of central (**A**) inferior and (**B**) superior retinal 1/T1 after manganese injection as a function of retinal depth for LA age-matched B6 (*black, n* = 6) and Cav1.2 L-type calcium channel BAY K 8644–insensitive mutant B6 mice (*green, n* = 5). Low-resolution MRI insert shows retina (*black line*) and the region studied (*white line*); a high-resolution image of the retina is shown in Figure 1. Representative images from the far left and far right side of the OCT image of a Cav1.2 L-type calcium channel BAY K 8644–insensitive mutant B6 mouse are shown above profiles; these OCT data were collected early in the study and may not represent a superior–inferior orientation. This lack of orientation is not expected to introduce substantial alignment error because OCT thicknesses are relatively homogenous across quadrants in mice,[112] and we find no differences in whole retinal thickness as measured on MRI between Cav1.2 L-type calcium channel BAY K 8644–insensitive mutant B6 mice (mean 216 μm [95% confidence limits 211–222 μm] versus wild-type mice thicknesses in Fig. 6). Approximate location of two anatomic landmarks is indicated by *dashed, vertical lines* (i.e., anterior aspect of the outer plexiform layer [*left*] and retina/choroid border [*right*]). *Range bar*: retinal depth range with significant difference (*P* < 0.05). *Error bars*: standard error of the mean.

that contain a point mutation causing a specific loss-of-function only to manipulation by the dihydropyridine BAY K 8644.[45,46] Each group was treated with BAY K 8644 dissolved in dimethyl sulfoxide (bolus intraperitoneal, 8 mg/kg; Sigma-Aldrich Corp., St. Louis, MO, USA) approximately 4 hours before examination. It is appreciated that unambiguous immunostaining antibody for Cav1.3 is needed and, in part because the *Cacna1* gene can generate multiple CaV channels by alternative splicing, is not currently feasible.[47] It is also appreciated that L-type channel knockout mice are problematic: globally knocking out Cav1.2 is fatal and other L-type calcium channel knockouts have known compensatory effects. For example, work from our lab and others find that knocking out Cav1.3 results in compensatory upregulation of Cav1.2.[25,48] Thus, the Cav1.2-dihydropyridine^{−/−} mice were a reasonable option for in vivo testing of our hypothesis.

Testing of the second knowledge gap involved the following three groups: (1) dark and (2) light-adapted male 2- to 3-month oxidative stress–sensitive male B6, and (3) dark-adapted oxidative stress–resistant male 129S6/SvEvTac (S6; Taconic
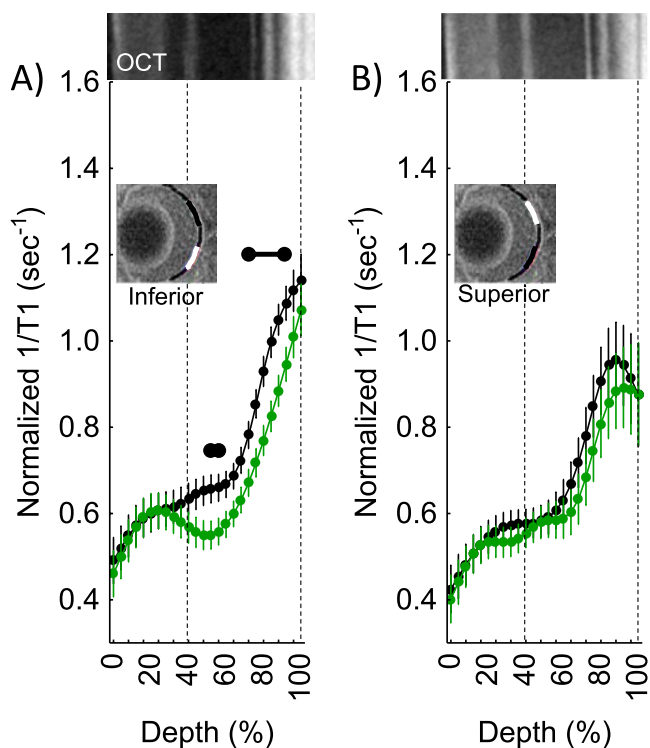

FIGURE 3. QUEST MRI measurements approximately 1-hour post d-*cis*-diltiazem in dark-adapted (DA) B6 mice. Modeling results of normalized 1/T1 MRI profiles in vivo for (**A**) inferior and (**B**) superior retina after administration of either saline (*black, n* = 7) or MB+ALA (*green, n* = 7) in different subgroups of mice. Other graphing conventions are described in the legend for Figure 2. Representative images from inferior and superior retina from OCT images of approximately 4-hours post DA B6 mice are shown above the approximately 1-hour post profiles. The use of OCT images from a different time point is not expected to introduce substantial alignment error because no differences were found in retinal thickness as measured on MRI between any of the post d-*cis*-diltiazem groups. Each 1/T1 data set was normalized to its TR 150 ms image ("normalized 1/T1"), as detailed in the Materials and Methods section.

Biosciences, Hudson, NY, USA) mice.[41] Each group was injected with d-*cis*-diltiazem dissolved in saline (bolus subcutaneously, 30 mg/kg; ≥ 99% purity; D-2521; Sigma-Aldrich Corp.), and subgroups examined 45 minutes to 1 hour 15 minutes (i.e., ~1 hour post), 1 hour 45 minutes to 2 hours 15 minutes (~2 hours post), or 3 hours 45 minutes to 4 hours 15 minutes (~4 hours post) after the injection.

Manganese-Enhanced MRI

MEMRI was used to test the mice for the first part of the study. Mice were maintained in darkness overnight and then exposed to room light for 15 to 20 minutes before injection of BAY K 8644 and then MnCl2 (intraperitoneal injection, 66 mg MnCl$_2$·4 H$_2$O/kg) 30 minutes later. Light hyperpolarizes rod membranes keeping the membrane-bound L-type calcium channels in a closed state. Application of BAY K 8644 opens closed L-type calcium channels resulting in an increased manganese influx. After injections, mice were maintained in room light for
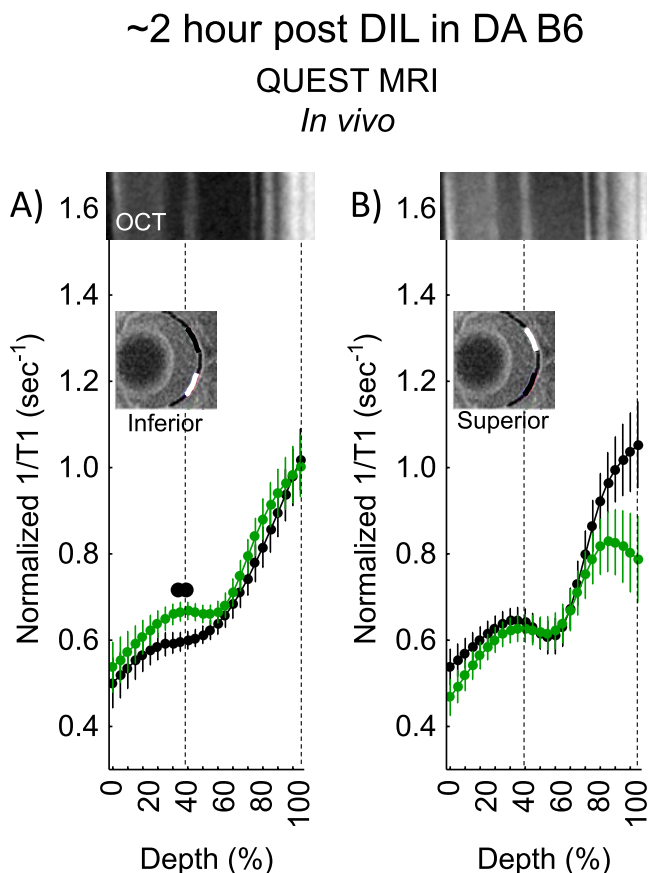
~2 hour post DIL in DA B6
QUEST MRI
In vivo

Figure 4. QUEST MRI measurements approximately 2-hours post d-*cis*-diltiazem in DA B6 mice. Modeling results of normalized 1/T1 MRI profiles in vivo for (**A**) inferior and (**B**) superior retina after administration of either saline (*black, n* = 5) or MB+ALA (*green, n* = 5) in different subgroups of mice. Other graphing conventions are described in the legend for Figures 2 and 3. Representative images from inferior and superior retina from OCT images of approximately 4-hours post DA B6 mice are shown above the approximately 2-hours post profiles. The use of OCT images from a different time point is not expected to introduce substantial alignment error because no differences were found in retinal thickness as measured on MRI between any of the post d-*cis*-diltiazem groups.

another 3.5 to 4 hours. High-resolution MRI data were acquired on a 7T system (ClinScan, Bruker, Billerica, MA, USA) using a receive-only surface coil (1.0-cm diameter) centered on the left eye. In all groups, immediately before the MRI experiment, animals were anesthetized with urethane (36% solution intraperitoneally; 0.083 mL/20 g animal weight, prepared fresh daily; Sigma-Aldrich Corp.) and treated topically with 1% atropine to ensure dilation of the iris during light exposure followed by 2% lidocaine gel to reduce eye motion. MEMRI data were acquired using several single spin-echo sequences (time to echo 13 ms, 7×7 mm^2, matrix size 160×320, slice thickness 600 μm). Images were acquired at different repetition times (TRs) in the following order (number per time between repetitions in parentheses): TR 0.15 seconds (6), 3.50 seconds (1), 1.00 seconds (2), 1.90 seconds (1), 0.35 seconds (4), 2.70 seconds (1), 0.25 seconds (5), and 0.50 seconds (3). To compensate for reduced signal–noise ratios at shorter TRs, progressively more images were collected as the TR decreased. The present resolution in the central retina is sufficient for extracting meaningful layer-specific anatomic and functional data, as previously discussed.[26]

QUEST MRI

Mice used for testing the second part of the study were maintained in darkness for at least 16 hours before as well as during the MRI examination. In all groups, immediately before the MRI experiment, animals were anesthetized with urethane and handled as described above. High-resolution 1/T1 data were acquired using the same procedure as above.

QUEST T1 data sets were collected from mice given d-*cis*-diltiazem either 45 minutes to 1 hour 15 minutes (i.e., ~1 hour post), 1 hour 45 minutes to 2 hours 15 minutes (~2 hours post), or 3 hours 45 minutes to 4 hours 15 minutes (~4 hours post) before QUEST examination. All mice were treated 24 hours prior to d-*cis*-diltiazem with 1 mg/kg MB (intraperitoneal, dissolved in saline) and then treated the next day approximately 1 hour before the second MRI examination with 50 mg/kg ALA (intraperitoneal, dissolved in saline and pH adjusted to ~7.4). MB is an alternate electron transporter that effectively suppresses generation of superoxide from a variety of sources; ALA is a potent free-radical neutralizer.[49,50] Control mice were also given d-*cis*-diltiazem as above, but followed with two saline injections instead of MB and ALA.

Retinal Superoxide Production

Subgroups of dark-adapted B6 and S6 mice were treated with d-*cis*-diltiazem approximately 4 hours before enucleation. These mice were maintained in darkness for at least 16 hours before euthanasia and retina removal. Superoxide production was measured on each retina using a standard lucigenin assay (bis-N-methylacridinium nitrate; Sigma-Aldrich Corp.).[43]

Optical Coherence Tomography

OCT (EnVisu R2200 VHR SDOIS OCT, Leica Microsystems, Wetzlar, Germany) was used to visualize retinal layer spacing in vivo in subgroups of mice (n = 2/group). Mice were anesthetized with urethane (36% solution intraperitoneally; 0.083 mL/20 g animal weight, prepared fresh daily; Sigma-Aldrich Corp.). One percent atropine sulfate was used to dilate the iris, and GenTeal (Novartis, Basel, Switzerland) was used to lubricate the eyes. OCT images were also used to visualize possible d-*cis*-diltiazem–evoked damage. Because representative OCT images are being compared with averaged MRI data, the location of two anatomic landmarks is approximate, and dashed vertical lines indicate key boundaries. Nonetheless, we have generated a body of work that confirms that aligning the vitreous–retina (0% depth) and retina–choroid (100% depth) borders of OCT and MRI images, as outlined in Figure 1, reasonably matches structure with function.[26]

MRI Data Analysis

For both MEMRI and QUEST data, each T1 data set of 23 images was first processed by registering (rigid body; STACKREG plugin, ImageJ; ImageJ software, http://imagej.nih.gov/ij/; provided in the public domain by the National Institutes of Health, Bethesda, MD, USA) and then averaging images with the same TRs in order to generate a stack of eight images. These averaged images were then registered (rigid body) across TRs. Because of its lower signal-to-noise compared with MEMRI, only QUEST data were corrected for imperfect slice profile bias in the estimate of T1 as previously described.[51] Briefly, normalizing to the shorter TR, some of the bias can be reduced giving a more precise estimate for T1. To achieve this normalization, we first apply a 3×3 Gaussian smoothing (performed 3 times) on only the TR 150-ms image to minimize noise and emphasize signal. The smoothed TR 150-ms image
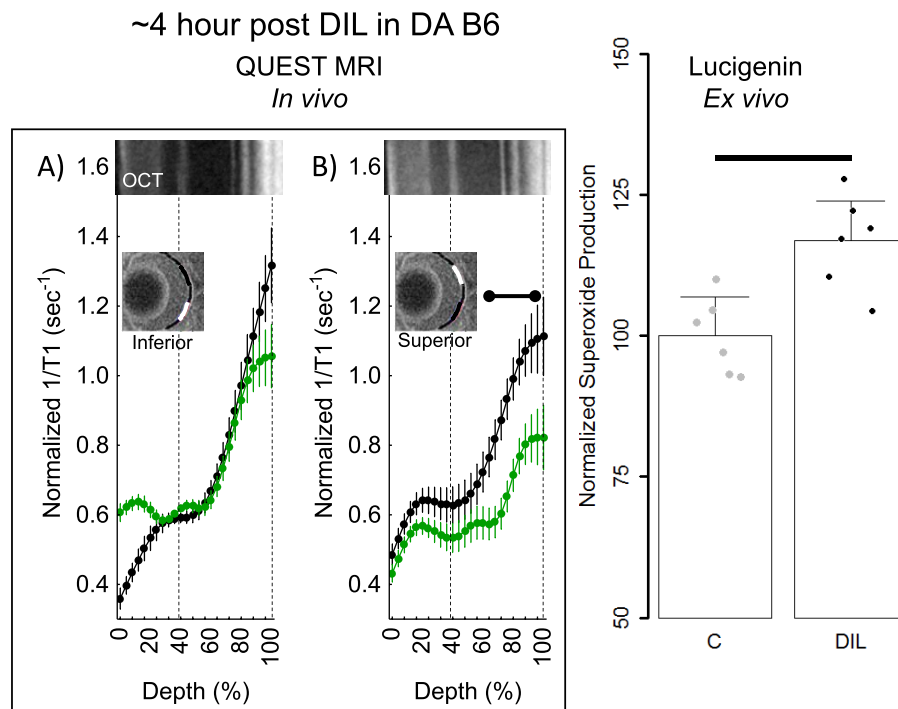
~4 hour post DIL in DA B6

FIGURE 5. QUEST MRI and superoxide measurements approximately 4-hours post d-*cis*-diltiazem in DA B6 mice. Modeling results of normalized 1/T1 MRI profiles in vivo for (**A**) inferior and (**B**) superior retina after administration of either saline (*black*, $n = 5$) or MB+ALA (*green*, $n = 7$), in different subgroups of mice. Other graphing conventions are described in the legend for Figures 2 and 3. (**C**) Modeled superoxide production measured on the same day from excised whole retinas from B6 ($n = 3$) and 4-hours post d-*cis*-diltiazem in B6 mice ($n = 3$). Individual data points (= number of eyes examined; one eye per mouse) represent the replicate average for each mouse to illustrate animal-to-animal variation; *error bars*: 95% confidence intervals. *Black bar* = significant difference ($P < 0.05$).

was then divided into the rest of the images in that T1 data set. Preliminary experiments (not shown) found that this procedure helps to minimize day-to-day variation in the 1/T1 profile previously noted and obviated the need for a "vanilla control" group used previously for correcting for day-to-day variations.[42,43] 1/T1 maps were calculated using the seven normalized images via fitting to a three-parameter T1 equation ($y = a + b \times (\exp [-c \times TR]$), where a, b, and c are fitted parameters) on a pixel-by-pixel basis using R (v.2.9.0, R Development Core Team, 2009; R Foundation for Statistical Computing, Vienna, Austria) scripts developed in-house, and the minpack.lm package (v.1.1.1, Timur V. Elzhov and Katharine M. Mullen minpack.lm: R interface to the Levenberg-Marquardt nonlinear least-squares algorithm found in MINPACK. R package version 1.1–1).

In each mouse, retinal thicknesses (µm) were objectively determined using the "half-height method," wherein a border is determined via a computer algorithm based on the crossing point at the midpoint between the local minimum and maximum, as detailed elsewhere.[52,53] The distance between two neighboring crossing points, thus represents an objectively defined retinal thickness. One/T1 profiles in each mouse were then normalized with 0% depth at the presumptive vitreoretinal border and 100% depth at the presumptive retina–choroid border (Fig. 1). The present resolution is sufficient for extracting meaningful layer-specific anatomic and functional data, as previously discussed (Fig. 1).[3,54]

Our usual analysis compared the averaged superior and inferior values from ±0.4 to 1 mm from the optic nerve head generated for each animal group. However, to better compare QUEST MRI data with that from the lucigenin assay

(which evaluates the entire retina) we expanded our analysis to include more peripheral retinal regions (±0.4–1.4 mm from the optic nerve head). In addition, upon consultation with a biostatistician (RP), we found that the two sides behaved differently (not shown), so each side was analyzed separately.

Statistical Analysis

Data are presented as mean ± SEM, and a significance level of 0.05 was used for all analyses. All of the outcomes (1/T1, retinal superoxide production, and MRI thickness) had repeated measures for each mouse. As such, we used mixed-linear models to analyze all of the outcomes, using the Kenward-Roger method for calculating degrees of freedom in SAS 9.4 (SAS Software, Cary, NC, USA). For the MRI profile data (1/T1), we used cubic splines to model and compare mouse-specific profiles between groups (SAS software). The number of "windows" with a relationship between 1/T1 and location (i.e., "knots") was initially evaluated separately for each group for any given analysis, and the Akaike and Schwarz Bayesian information criteria (AIC and BIC) were used to identify the model with the fewest knots needed to model all groups. Random coefficients for the intercept and the location-specific coefficients (cubic spline coefficients) were also evaluated using AIC and BIC. The model included the fixed effects of strain, antioxidant treatment, location-specific values for the cubic splines, and up to three-way interactions among the main effects. Higher-order interactions were removed from the model if they were not significant at the 0.05 level. To calculate a total antioxidant effect across the entire profile, we summed
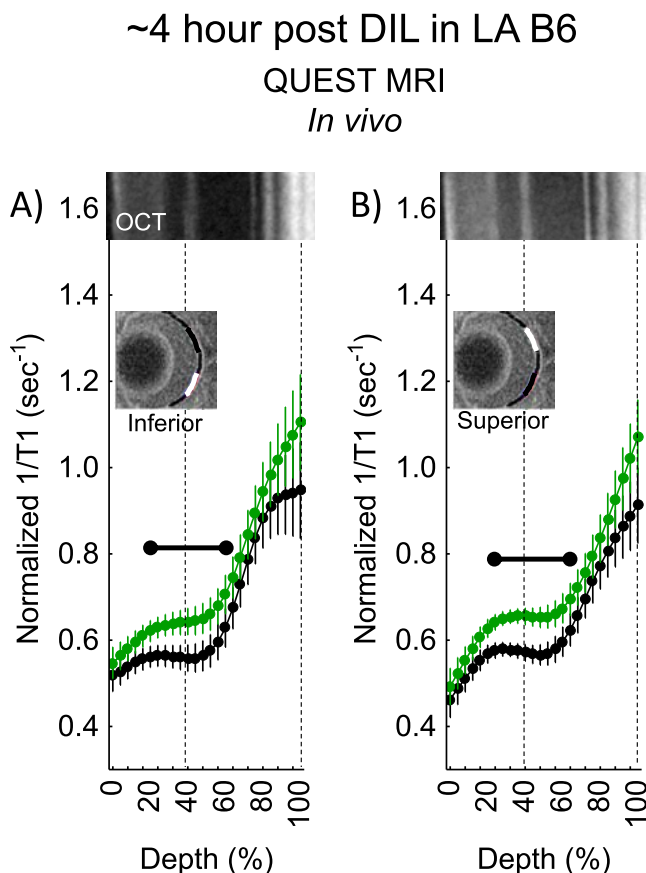
~4 hour post DIL in LA B6
QUEST MRI
In vivo

FIGURE 6. QUEST MRI measurements approximately 4-hours post d-*cis*-diltiazem in LA B6 mice. Modeling results of normalized 1/T1 MRI profiles in vivo for (**A**) inferior and (**B**) superior retina after administration of either saline (*black*, n = 5) or MB+ALA (*green*, n = 4) in different subgroups of mice. Other graphing conventions are described in the legend for Figures 2 and 3. Representative images from inferior and superior retina from OCT images of approximately 4-hours post DA B6 mice are shown above the approximately 4-hour LA B6 profiles. The use of OCT images from a different light condition is not expected to introduce substantial alignment error because no differences were found in retinal thickness as measured on MRI between any of the post d-*cis*-diltiazem groups.

the predicted values for the appropriate interaction across all locations.

Retinal superoxide production was analyzed using a model that included the fixed effect of treatment, and the random effects of mouse within treatment and "shake" within mouse and treatment (each mouse's sample was shaken, measured three times, and the process repeated 3–4 times).

Thickness was analyzed using a mixed-linear model with the fixed effects of group and side (superior and inferior) and a random intercept for each mouse nested within group.

RESULTS

Testing Mouse Rods for Cav1.2 L-Type Calcium Channels

Manganese uptake in inferior retina (at 4%–60% retinal depth from the vitreous–retina boundary) and superior retina (at 24%–52% retinal depth) were less responsive ($P < 0.05$) to systemic BAY K 8644 in Cav1.2dihydropyridine^{−/−} mice than in control B6 mice (Fig. 2); a small region of superior retina at 72% to 80% depth into

the retina was relatively more responsive ($P < 0.05$) in mutant mice than controls. The regions from mutant mice with a subnormal BAY K 8644 response indicate the location of Cav1.2 L-type calcium channels; the relatively more responsive region may indicate compensatory overexpression of another L-type calcium channel in the outer retina (i.e., Cav1.3.[6,55]). In addition, the retinal ganglion cell and inner plexiform layers of inferior retina of Cav1.2dihydropyridine^{−/−} mice were unresponsive to BAY K 8644, whereas this was not the case for superior retina (Fig. 2).

Testing Whether d-*cis*-Diltiazem Modifies Rod Redox Environment

In this section, the method that has been validated to represent excessive production of reactive oxygen species is a 1/T1 that is significantly reduced with antioxidant injection compared with saline injection (i.e., a positive QUEST MRI response).[41–44] Regions that show a significantly increased response to antioxidants are not considered to indicate excessive production of reactive oxygen species because this increased response has no theoretic or biophysical basis linking it with oxidative stress. For this reason, significant increases with antioxidant exposure are not indicated on the graphs for clarity.

D-*cis*-Diltiazem–Induced Oxidative Stress

Dark-adapted B6 mice approximately 1-hour post d-*cis*-diltiazem showed a positive QUEST MRI response indicative of excessive production of reactive oxygen species in most of the outer inferior retina, but not in superior retina (Fig. 3). By approximately 2 hours post, a positive response was observed, but only in a small region of inner inferior retina (Fig. 4). By approximately 4 hours post, the entire outer retina of superior (but not inferior outer retina) showed evidence for a positive response (Fig. 5).

Because approximately 4 hours post had the largest spatial burden of oxidative stress (e.g., compare positive responses in Figs. 3, 5), we focused on this time point for the rest of the studies. First, using a gold-standard lucigenin assay at approximately 4-hours post d-*cis*-diltiazem in dark-adapted B6 mice, a supernormal response was observed, consistent with the presence of oxidative stress in the total retina (Fig. 5). Next, we asked if d-*cis*-diltiazem could induce a positive QUEST MRI response approximately 4-hours post d-*cis*-diltiazem injection if the mice were light- instead of dark-adapted. As shown in Figure 6, no evidence for a positive response was noted in light-adapted d-*cis*-diltiazem–treated B6 mice; however, there are regions showing a supernormal response ($P < 0.05$; not indicated on the graph). Because dark-adapted S6 mice were oxidative stress–resistant following a pharmacologic insult (sodium iodate[41]), we asked if these mice are also resistant to d-*cis*-diltiazem–evoked excessive production of reactive oxygen species. Indeed, approximately 4-hours post d-*cis*-diltiazem, dark-adapted S6 mice showed neither a positive QUEST response nor supernormal production of superoxide free radicals (Fig. 7).

Retinal Thickness

As shown in Figure 8, no evidence for retinal thinning was found in any d-*cis*-diltiazem–treated group.

DISCUSSION

In this study, we address knowledge gaps about d-*cis*-diltiazem's interaction with normal murine rod cells in vivo
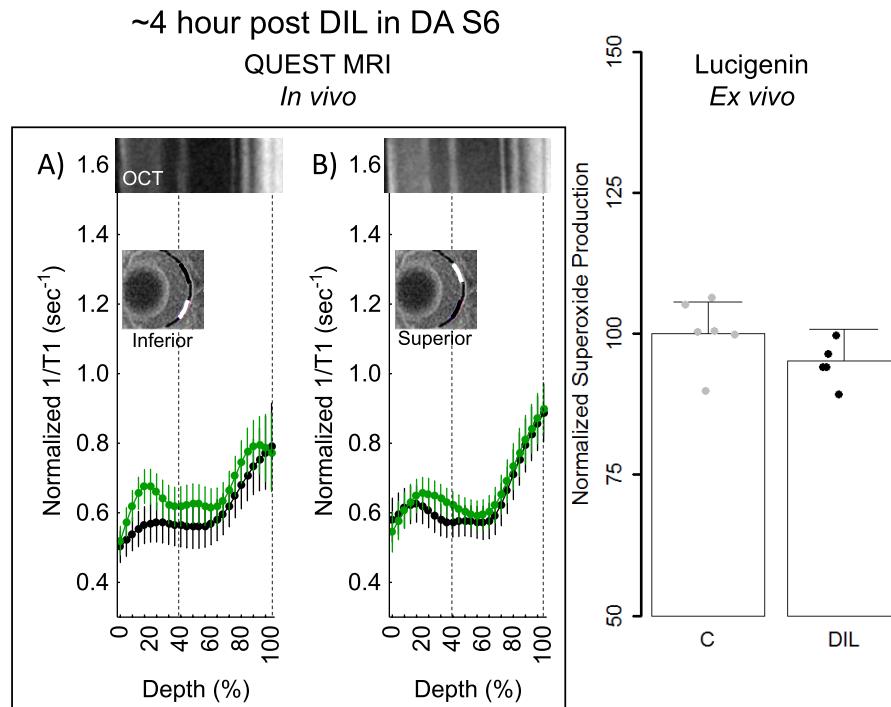
FIGURE 7. QUEST MRI and superoxide measurements approximately 4-hours post d-*cis*-diltiazem in DA S6 mice. Modeling results of normalized 1/T1 MRI profiles in vivo for (**A**) inferior and (**B**) superior retina after administration of either saline (*black*, $n = 5$) or MB+ALA (*green*, $n = 6$) in different subgroups of mice. Other graphing conventions are described in the legend for Figures 2 and 3. Representative images from inferior and superior retina from OCT images of approximately 4-hours post DA B6 mice are shown above the S6 hour post profiles. The use of OCT images from a different time point is not expected to introduce substantial alignment error because no differences were found in retinal thickness as measured on MRI between any of the groups, also, no differences in retinal layer spacing was previously reported on OCT images of B6 and S6 mice.[41] (**C**) Modeled superoxide production normalized to same day controls from excised whole retinas from S6 ($n = 6$) and 4-hours post d-*cis*-diltiazem in S6 mice ($n = 5$). Individual data points (= number of eyes examined; one eye per mouse) represent the replicate average for each mouse to illustrate animal-to-animal variation; *error bars*: 95% confidence intervals. *Black bar* = significant difference ($P < 0.05$).

to potentially improve our comprehension of decades of contradictory reports on its neuroprotective effects in RP models.[6,56,57] Because calcium overload precedes photoreceptor degeneration, it is important to understand outer retinal calcium regulation via, for example, L-type calcium channels (a major influx pathway).[58] D-*cis*-Diltiazem is a blocker of Cav1.2 L-type calcium channels.[10,56] However, there has been uncertainty about these channels in vivo in the healthy young murine outer retina based on differing findings in immunohistochemical, pharmacologic, and electrophysiologic transretinal maps of Cav1.2 L-type calcium channels.[3,6,10,23,58–60] For example, antibodies for L-type calcium channel are problematic and produce different results for Cav1.2 channel expression in the inner retina of rodents.[60–62] Also, no good immunostaining antibodies for Cav1.3 channels exist.[61] Furthermore, several ex vivo investigations involving bovine, salamander, and porcine photoreceptors, or in mice that have retinas that degenerate (rd1 mice), find evidence that photoreceptors in the outer retina are responsive to d-*cis*-diltiazem and that synaptic photoreceptor L-type voltage-gated Ca2+ channels are a target for d-*cis*-diltiazem.[7,10,16,23,24] In contrast, in 2- to 5-month B6 mice, the inner, but not outer, retina in vivo was reported to be responsive to systemic d-*cis*-diltiazem treatment.[3] It has not been clear how to reconcile these ex vivo and in vivo data. This may be due to the age or strain of mice because d-*cis*-diltiazem has been found to reduce uptake of manganese in outer retina in older B6 mice, in Cav1.3 knockout mice, and in rats.[3,4,25] However, in the present study, using a genetic approach, we unambiguously identify in vivo functional Cav1.2 L-type calcium channels in

both inner and outer retina of 2- to 3-month male mice based on results obtained from a unique combination of in vivo imaging of L-type calcium channel function (MEMRI) and mice modified to be unresponsive to the dihydropyridine agonist BAY K 8644. Mouse retina contain approximately 97% rod photoreceptors making the contribution of cone uptake of manganese too small to substantially alter the interpretation of the results.[63] One possible explanation for why d-*cis*-diltiazem was not reported to be effective in outer retina in young mice is that the outer retina contains nonconventional Cav1.2 L-type calcium channels.[10,23] Together, the above considerations support the presence of d-*cis*-diltiazem-insensitive Cav1.2 L-type calcium channels in 2- to 5-month male mouse outer retina. More work in this area is needed, including studies in female mice.

In the second part of this study, we provide evidence that d-*cis*-diltiazem evoked excessive production of reactive oxygen species in dark-adapted rod cells in vivo, an effect previously reported only (to our knowledge) in nonretinal tissue and cells.[35–40] Importantly, we find a complex spatiotemporal picture that reflects the unique ability of QUEST MRI to noninvasively provide both high-spatial and high-temporal resolution (i.e., a "snapshot" in time) regarding excessive production of reactive oxygen species. We and others have confirmed the underlying physics behind QUEST MRI: a continuous net production of free radicals (i.e., oxidative stress) that generates a robust and detectable T1 contrast mechanism consistent with inherently paramagnetic free radicals shortening the lifetime (i.e., T1) of water protons, causing 1/T1 to increase linearly based on the concentration of
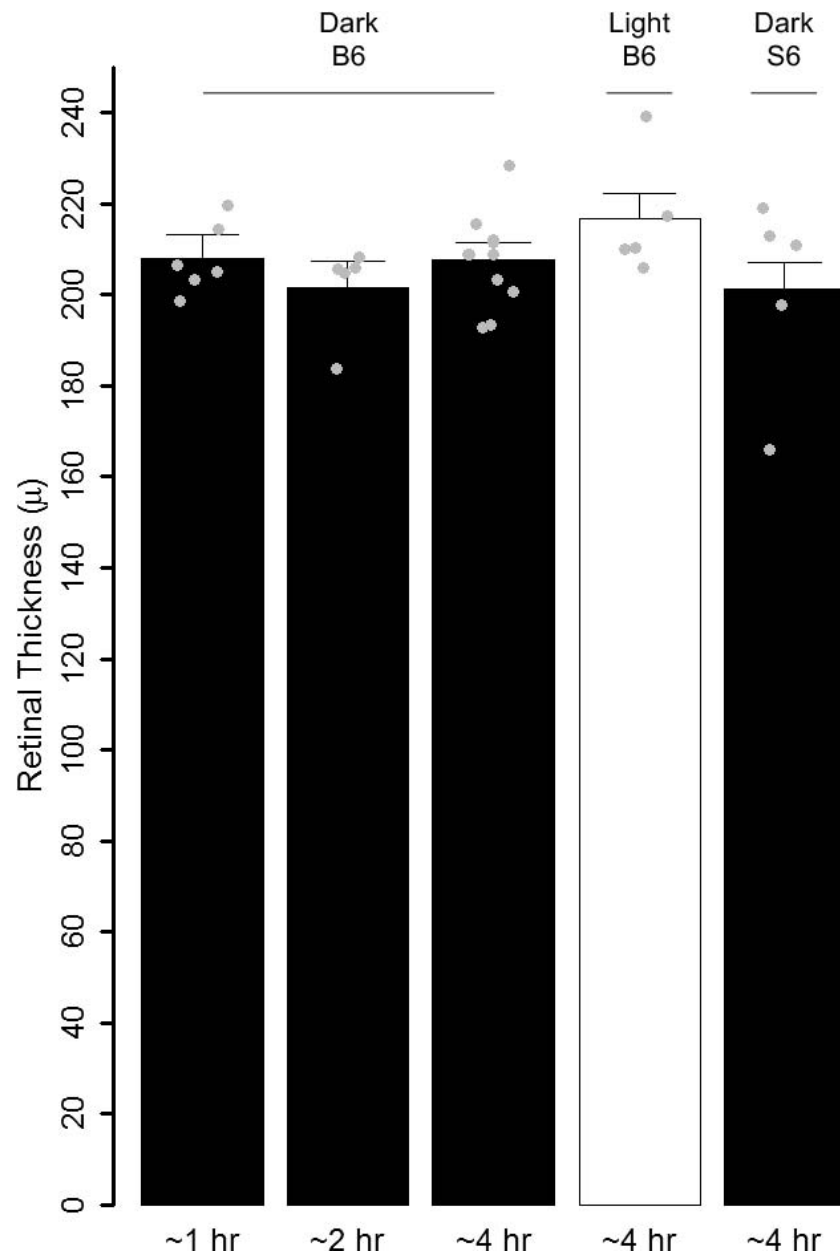
FIGURE 8. Summary of averaged inferior and superior MRI retinal thickness as measured from d-*cis*-diltiazem–treated groups after saline injection. Individual data points (= number of eyes examined; one eye per mouse) represent the replicate average for each mouse to illustrate animal-to-animal variation; *error bars*: 95% confidence intervals.

the paramagnetic agent.[42–44,64–66] The underlying physics has been validated in the xanthine–xanthine oxidase reaction ex vivo and in several different models of neuronal oxidative stress.[42–44,64–66] For these reasons, our observation of oxidative stress in photoreceptors following d-*cis*-diltiazem based on QUEST MRI is reasonable.

In this study, a common lucigenin assay was used to quantitatively measure a snapshot of retinal free-radical production. A major source of free radicals are mitochondria, and approximately 75% of retinal mitochondria are in photoreceptor cells.[67] It is not unreasonable to speculate that photoreceptors are implicated in the superoxide generation measured using the lucigenin assay of the retina, but confirming this requires further experiments. We considered testing the QUEST MRI results against conventional histologic markers of oxidative stress, such as 4-hydroxynonenal or 8-oxo-

guanine. One problem with these histologic markers is that they are not a direct measure of free-radical production but rather only qualitatively visualize oxidative damage, a footprint of long-standing oxidative stress. In this study, d-*cis*-diltiazem is administered acutely with oxidative stress appearing transiently in different retinal regions and with normalization of indices by 24-hours post d-*cis*-diltiazem (preliminary data not shown). For these reasons, histologic endpoints of oxidative damage that result from prolonged oxidative stress were not used in this study.

The present results raise the possibility that different mechanisms underlie d-*cis*-diltiazem's temporally distinct excessive production of reactive oxygen species in inferior and superior retina. While not a focus of the present study, we speculate about two potential mechanisms by which d-*cis*-diltiazem can promote excessive production of reactive oxygen

species. The first possible mechanism is based on the fact that diltiazem undergoes oxidative metabolism in the liver by cytochrome P450 enzymes, and cytochrome P450 can give rise to excessive production of reactive oxygen species.[68,69] New research has identified cytochrome P450 activity in photoreceptor and other retinal cells, and in the brain, raising the possibility of xenobiotic cytochrome P450-based excessive production of reactive oxygen species.[69–74] It is not yet known if photoreceptors in inferior retina contain more cytochrome P450 activity than in superior retina, but this is a testable hypothesis for future studies. A second possible mechanism (not mutually exclusive with the cytochrome P450 hypothesis) may involve the ability of d-*cis*-diltiazem to modify dark-adapted photoreceptor cell calcium homeostasis, because cell calcium dysregulation can lead to oxidative stress.[26,56,75,76] Given the large role light plays in photoreceptor calcium regulation and lack of evidence that mammalian photoreceptor cytochrome P450 activity is light dependent, it is intriguing that excessive production of reactive oxygen species was not produced approximately 4-hours post d-*cis*-diltiazem in light-adapted B6 mice. An oxygen consumption rate measurement on retinal tissue punches is a potentially powerful method to interrogate the reserve capacity of photoreceptor mitochondria and may be considered in a potential follow-up study, but is not necessary to address the goals of this study.[77] More work is needed in male and female mice to unravel the underlying mechanism of rod cell excessive production of reactive oxygen species in vivo.

In the present study, we noted that dark-adapted B6 and S6 male mice had different excessive production of reactive oxygen species responses to d-*cis*-diltiazem at approximately 4 hours post.[41] This observation is consistent with previous studies that show that genetic differences between strains can generate distinct oxidative stress vulnerabilities due to differences in cytochrome P450 transcript levels and are known to modify photoreceptor oxidative stress defenses against various insults, such as sodium iodate.[41,78,79] Further investigation is needed to investigate each possibility in more detail.

In this study, we observed substantial inferior–superior topographic variations in inner retinal Cav1.2 L-type calcium channel function and in outer retinal excessive production of reactive oxygen species pattern following d-*cis*-diltiazem. In a healthy retina, previous research has found a range of inferior–superior variations, such as (but not limited to) approximately 20% longer rod outer segments in superior versus inferior retina.[80–89] Also, in some disease models, relatively more outer retinal abnormalities/degeneration have been reported in inferior retina than in superior retina, but in other models, the opposite pattern is found.[90–96] Despite decades of research, it remains unclear exactly how hemiretinal differences develop and progress over time.[83,86,97–99] Nonetheless, within presumably homogenous populations of neurons there is considerable within-class heterogeneity.[100] The present results, and a recent report suggesting region-specific oxidative stress susceptibilities in humans,[101] support this notion with evidence of an inferior-to-superior gradient of rod cell functionality and susceptibility to oxidative stress. In the context of RP, a spatial oxidative stress vulnerability gradient in outer retina may be important given the observation in an RP model that cones tend to survive better in the inferior retina compared with superior retina.[93] More work is needed to further explore this notion.

Improving antioxidant treatment efficacy against outer retinal degenerative disease is expected to require identifying individuals who are most susceptible to excessive production of reactive oxygen species. In experimental studies, a toxic oxidizing agent is usually given to test retinal oxidative stress tolerance before photoreceptor atrophy.[41,78,102–104] For example, sodium iodate produces more outer retinal loss and excessive production of reactive oxygen species in B6 mice than in S6 mice.[41] Measuring an evoked retinal oxidative stress response in patients may be useful for future personalization of antioxidant treatment efficacy as long as the evoked response is nontoxic. Because d-*cis*-diltiazem is FDA approved and commonly used clinically, the present results raise the possibility that d-*cis*-diltiazem might be useful for testing individuals for oxidative stress susceptibility without producing retinal damage and for evaluating the efficacy of new antioxidant treatments. These tests could take advantage of QUEST MRI's measurement of excessive production of reactive oxygen species without a contrast agent, giving it strong translational potential.

In summary, the present results raise the possibility that d-*cis*-diltiazem–induced outer retinal oxidative stress may be a confounding factor in the context of the controversial results following d-*cis*-diltiazem treatment for RP. Because oxidative stress is a trigger of photoreceptor atrophy, it can also act as a prosurvival preconditioning, and therefore this potentially confounding response deserves more attention than it has received thus far.[91,105–109]

References

1. Baumann L, Gerstner A, Zong X, Biel M, Wahl-Schott C. Functional characterization of the L-type Ca2+ channel Cav1.4a1 from mouse retina. *Invest Ophthalmol Vis Sci*. 2004;45:708–713.

2. Tarabova B, Lacinova L, Engel J. Effects of phenylalkylamines and benzothiazepines on Cav1.3-mediated Ca2+ currents in neonatal mouse inner hair cells. *Eur J Pharmacol*. 2007;573:39–48.

3. Berkowitz BA, Grady EM, Roberts R. Confirming a prediction of the calcium hypothesis of photoreceptor aging in mice. *Neurobiol Aging*. 2014;35:1883–1891.

4. Bissig D, Goebel D, Berkowitz BA. Diminished vision in healthy aging is associated with increased retinal L-type voltage gated calcium channel ion influx. *PLoS One*. 2013;8:e56340.

5. Glossmann H, Linn T, Rombusch M, Ferry DR. Temperature-dependent regulation of d-cis-[3H]diltiazem binding to Ca2+ channels by 1,4-dihydropyridine channel agonists and antagonists. *FEBS Lett*. 1983;160:226–232.

6. Shi L, Chang JY-A, Yu F, Ko ML, Ko GY-P. The contribution of L-type Cav1.3 channels to retinal light responses. *Front Mol Neurosci*. 2017;10:394.

7. Frasson M, Sahel JA, Fabre M, Simonutti M, Dreyfus H, Picaud S. Retinitis pigmentosa: rod photoreceptor rescue by a calcium-channel blocker in the rd mouse. *Nat Med*. 1999;5:1183–1187.

8. Sanges D, Comitato A, Tammaro R, Marigo V. Apoptosis in retinal degeneration involves cross-talk between apoptosis-inducing factor (AIF) and caspase-12 and is blocked by calpain inhibitors. *Proc Natl Acad Sci U S A*. 2006;103: 17366–17371.

9. Read DS, McCall MA, Gregg RG. Absence of voltage-dependent calcium channels delays photoreceptor degeneration in rd mice. *Exp Eye Res*. 2002;75:415–420.

10. Cia D, Bordais A, Varela C, et al. Voltage-gated channels and calcium homeostasis in mammalian rod photoreceptors. *J Neurophysiol*. 2005;93:1468–1475.

11. Vallazza-Deschamps G, Cia D, Gong J, et al. Excessive activation of cyclic nucleotide-gated channels contributes to neuronal degeneration of photoreceptors. *Eur J Neurosci*. 2005;22:1013–1022.

12. Fox DA, Poblenz AT, He L. Calcium overload triggers rod photoreceptor apoptotic cell death in chemical-induced and inherited retinal degenerations. *Ann N Y Acad Sci*. 1999;893: 282–285.

13. Nakazawa M. Effects of calcium ion, calpains, and calcium channel blockers on retinitis pigmentosa. *J Ophthalmol*. 2011;2011:292040.

14. Schön C, Paquet-Durand F, Michalakis S. Ca(v)1.4 L-type calcium channels contribute to calpain activation in degenerating photoreceptors of rd1 Mice. *PLoS One*. 2016; 11:e0156974.

15. Pasantes-Morales H, Quiroz H, Quesada O. Treatment with taurine, diltiazem, and vitamin E retards the progressive visual field reduction in retinitis pigmentosa: a 3-year follow-up study. *Metab Brain Dis*. 2002;17:183–197.

16. Pawlyk BS, Li T, Scimeca MS, Sandberg MA, Berson EL. Absence of photoreceptor rescue with d-cis-diltiazem in the rd mouse. *Invest Ophthalmol Vis Sci*. 2002;43:1912–1915.

17. Bush RA, Kononen L, Machida S, Sieving PA. The effect of calcium channel blocker diltiazem on photoreceptor degeneration in the rhodopsin Pro23His rat. *Invest Ophthalmol Vis Sci*. 2000;41:2697–2701.

18. Ma EY, Lewis A, Barabas P, et al. Loss of Pde6 reduces cell body Ca(2+) transients within photoreceptors. *Cell Death Dis*. 2013;4:e797.

19. Pearce-Kelling SE, Aleman TS, Nickle A, et al. Calcium channel blocker D-cis-diltiazem does not slow retinal degeneration in the PDE6B mutant rcd1 canine model of retinitis pigmentosa. *Mol Vis*. 2001;7:42–47.

20. Yamazaki H, Ohguro H, Maeda T, et al. Preservation of retinal morphology and functions in Royal College Surgeons rat by nilvadipine, a Ca2+ antagonist. *Invest Ophthalmol Vis Sci*. 2002;43:919–926.

21. Takano Y, Ohguro H, Dezawa M, et al. Study of drug effects of calcium channel blockers on retinal degeneration of rd mouse. *Biochem Biophys Res Commun*. 2004;313:1015–1022.

22. Usui S, Oveson BC, Lee SY, et al. NADPH oxidase plays a central role in cone cell death in retinitis pigmentosa. *J Neurochem*. 2009;110:1028–1037.

23. Hart J, Wilkinson MF, Kelly MEM, Barnes S. Inhibitory action of diltiazem on voltage-gated calcium channels in cone photoreceptors. *Exp Eye Res*. 2003;76:597–604.

24. Koch KW, Kaupp UB. Cyclic GMP directly regulates a cation conductance in membranes of bovine rods by a cooperative mechanism. *J Biol Chem*. 1985;260:6788–6800.

25. Berkowitz BA, Murphy GG, Craft CM, Surmeier DJ, Roberts R. Genetic dissection of horizontal cell inhibitory signaling in mice in complete darkness in vivo. *Invest Ophthalmol Vis Sci*. 2015;56:3132–3139.

26. Berkowitz BA, Bissig D, Roberts R. MRI of rod cell compartment-specific function in disease and treatment in svivo. *Prog Retin Eye Res*. 2016;51:90–106.

27. Ramos de Carvalho JE, Verbraak FD, Aalders MC, van Noorden CJ, Schlingemann RO. Recent advances in ophthalmic molecular imaging. *Surv Ophthalmol*. 2014;59:393–413.

28. Sinnegger-Brauns MJ, Huber IG, Koschak A, et al. Expression and 1,4-dihydropyridine-binding properties of brain l-type calcium channel isoforms. *Mol Pharmacol*. 2009;75:407–414.

29. Sinnegger-Brauns MJ, Hetzenauer A, Huber IG, et al. Isoform-specific regulation of mood behavior and pancreatic beta cell and cardiovascular function by L-type Ca 2+ channels. *J Clin Invest*. 2004;113:1430–1439.

30. Kang K, Tarchick MJ, Yu X, Beight C, Bu P, Yu M. Carnosic acid slows photoreceptor degeneration in the Pde6b(rd10) mouse model of retinitis pigmentosa. *Sci Rep*. 2016;6:22632.

31. Oveson BC, Iwase T, Hackett SF, et al. Constituents of bile, bilirubin and TUDCA, protect against oxidative stress-induced retinal degeneration. *J Neurochem*. 2011;116:144–153.

32. Galbinur T, Obolensky A, Berenshtein E, et al. Effect of para-aminobenzoic acid on the course of retinal degeneration in the rd10 mouse. *J Ocul Pharmacol Ther*. 2009;25:475–482.

33. Shen J, Yang X, Dong A, et al. Oxidative damage is a potential cause of cone cell death in retinitis pigmentosa. *J Cell Physiol*. 2005;203:457–464.

34. Yu DY, Cringle S, Valter K, Walsh N, Lee D, Stone J. Photoreceptor death, trophic factor expression, retinal oxygen status, and photoreceptor function in the P23H rat. *Invest Ophthalmol Vis Sci*. 2004;45:2013–2019.

35. Rajaraman G, Wang G, Smith HJ, Gong Y, Burczynski FJ. Effect of diltiazem isomers and thiamine on piglet liver microsomal peroxidation using dichlorofluorescein. *J Pharm Pharm Sci*. 2007;10:380–387.

36. Castro J, Hughes R, Smith H, Barritt GJ. Diltiazem protects hepatocytes from damage induced by reactive oxygen species through actions on mitochondria. *J Gastroenterol Hepatol Res*. 2016:5:1977–1983.

37. Velena A, Zarkovic N, Gall Troselj K, et al. 1,4-dihydropyridine derivatives: dihydronicotinamide analogues—model compounds targeting oxidative stress. *Oxid Med Cell Longev*. 2016;2016:1892412.

38. Morakinyo A, Iranloye B, Adegoke O. Calcium antagonists modulate oxidative stress and acrosomal reaction in rat spermatozoa. *Arch Med Sci*. 2011;7:613–618.

39. Okwa IB, Akindele AJ, Agbaje EO, Oshinuga OT, Anunobi CC, Adeyemi OO. Effect of subclinical, clinical and supra-clinical doses of calcium channel blockers on models of drug-induced hepatotoxicity in rats. *EXCLI J*. 2013;12:231–250.

40. Farghali H, Kmonickova E, Lotkova H, Martinek J. Evaluation of calcium channel blockers as potential hepatoprotective agents in oxidative stress injury of perfused hepatocytes. *Physiol Res*. 2000;49:261–268.

41. Berkowitz BA, Podolsky RH, Lenning J, et al. Sodium iodate produces a strain-dependent retinal oxidative stress response measured in vivo using QUEST MRI. *Invest Ophthalmol Vis Sci*. 2017;58:3286–3293.

42. Berkowitz BA, Lewin AS, Biswal MR, Bredell BX, Davis C, Roberts R. MRI of retinal free radical production with laminar resolution in vivo. *Invest Ophthalmol Vis Sci*. 2016; 57:577–585.

43. Berkowitz BA, Bredell BX, Davis C, Samardzija M, Grimm C, Roberts R. Measuring in vivo free radical production by the outer retina. *Invest Ophthalmol Vis Sci*. 2015;56:7931–7938.

44. Berkowitz BA, Lenning J, Khetarpal N, et al. In vivo imaging of prodromal hippocampus CA1 subfield oxidative stress in models of Alzheimer disease and Angelman syndrome. *FASEB J*. 2017;31:4179–4186.

45. Striessnig J, Koschak A, Sinnegger-Brauns MJ, et al. Role of voltage-gated L-type Ca2+ channel isoforms for brain function. *Biochem Soc Trans*. 2006;34:903–909.

46. Zhang J, Berra-Romani R, Sinnegger-Brauns MJ, Striessnig J, Blaustein MP, Matteson DR. Role of Cav1.2 L-type Ca2+ channels in vascular tone: effects of nifedipine and Mg2+. *Am J Physiol Heart Circ Physiol*. 2007;292:H415–H425.

47. Lipscombe D, Andrade A, Allen SE. Alternative splicing: functional diversity among voltage-gated calcium channels and behavioral consequences. *Biochim Biophys Acta*. 2013; 1828:1522–1529.

48. Jurkovicova-Tarabova B, Griesemer D, Pirone A, Sinnegger-Brauns MJ, Striessnig J, Friauf E. Repertoire of high voltage-activated Ca2+ channels in the lateral superior olive: functional analysis in wild-type, Ca(v)1.3(-/-), and Ca(v)1.2DHP(-/-) mice. *J Neurophysiol*. 2012;108:365–379.

49. Oz M, Lorke DE, Hasan M, Petroianu GA. Cellular and molecular actions of Methylene Blue in the nervous system. *Med Res Rev*. 2011;31:93–117.

50. Packer L. Antioxidant properties of lipoic acid and its therapeutic effects in prevention of diabetes complications and cataracts. *Ann N Y Acad Sci*. 1994;738:257–264.

51. Haacke EM, Brown RW, Thompson MR, Venkatesan R. *Magnetic Resonance Imaging: Physical Principles and Sequence Design*. New York: Wiley; 1999.

52. Bissig D, Berkowitz BA. Same-session functional assessment of rat retina and brain with manganese-enhanced MRI. *NeuroImage*. 2011;58:749–760.

53. Cheng H, Nair G, Walker TA, et al. Structural and functional MRI reveals multiple retinal layers. *Proc Natl Acad Sci U S A*. 2006;103:17525–17530.

54. Berkowitz BA, Grady EM, Khetarpal N, Patel A, Roberts R. Oxidative stress and light-evoked responses of the posterior segment in a mouse model of diabetic retinopathy. *Invest Ophthalmol Vis Sci*. 2015;56:606–615.

55. Xiao H, Chen X, Steele EC Jr. Abundant L-type calcium channel Ca(v)1.3 (alpha1D) subunit mRNA is detected in rod photoreceptors of the mouse retina via in situ hybridization. *Mol Vis*. 2007;13:764–771.

56. Fox DA, Poblenz AT, He L, Harris JB, Medrano CJ. Pharmacological strategies to block rod photoreceptor apoptosis caused by calcium overload: a mechanistic target-site approach to neuroprotection. *Eur J Ophthalmol*. 2003;13(Suppl 3):S44–S56.

57. Barabas P, Cutler PC, Krizaj D. Do calcium channel blockers rescue dying photoreceptors in the Pde6b (rd1) mouse? *Adv Exp Med Biol*. 2010;664:491–499.

58. Ko ML, Liu Y, Dryer SE, Ko GY-P. The expression of L-type voltage-gated calcium channels in retinal photoreceptors is under circadian control. *J Neurochem*. 2007;103:784–792.

59. Firth SI, Morgan IG, Boelen MK, Morgans CW. Localization of voltage-sensitive L-type calcium channels in the chicken retina. *Clin Exp Ophthalmol*. 2001;29:183–187.

60. Xu HP, Zhao JW, Yang XL. Expression of voltage-dependent calcium channel subunits in the rat retina. *Neurosci Lett*. 2002;329:297–300.

61. Zou J, Lee A, Yang J. The expression of whirlin and Cav1.3a1 is mutually independent in photoreceptors. *Vision Res*. 2012;75:53–59.

62. Busquet P, Khoi Nguyen N, Schmid E, et al. CaV1.3 L-type Ca2+ channels modulate depression-like behaviour in mice independent of deaf phenotype. *Int J Neuropsychopharmacol*. 2010;13:499–513.

63. Carter-Dawson LD, Lavail MM, Sidman RL. Differential effect of the rd mutation on rods and cones in the mouse retina. *Invest Ophthalmol Vis Sci*. 1978;17:489–498.

64. Tain RW, Scotti AM, Li W, Zhou XJ, Cai K. Imaging short-lived reactive oxygen species (ROS) with endogenous contrast MRI. *J Magn Reson Imaging*. 2018;47:222–229.

65. Stinnett G, Moore K, Samuel E, et al. A novel assay for the in vivo detection of reactive oxygen species using MRI. *ISMRM Meeting Abstracts*. 2015;1917.

66. Bakalova R, Georgieva E, Ivanova D, Zhelev Z, Aoki I, Saga T. Magnetic resonance imaging of mitochondrial dysfunction and metabolic activity, accompanied by overproduction of superoxide. *ACS Chem Neurosci*. 2015;6:1922–1929.

67. Johnson JE Jr, Perkins GA, Giddabasappa A, et al. Spatiotemporal regulation of ATP and Ca2+ dynamics in vertebrate rod and cone ribbon synapses. *Mol Vis*. 2007;13:887–919.

68. Molden E, Johansen PW, Boe GH, et al. Pharmacokinetics of diltiazem and its metabolites in relation to CYP2D6 genotype. *Clin Pharmacol Ther*. 2002;72:333–342.

69. Zangar RC, Davydov DR, Verma S. Mechanisms that regulate production of reactive oxygen species by cytochrome P450. *Toxicol Appl Pharmacol*. 2004;199:316–331.

70. Lee Y-H, Lee M-H, Shim C-K. Pharmacokinetics of diltiazem and deacetyldiltiazem in rats. *Int J Pharm*. 1991;76:71–76.

71. Nakano M, Lockhart CM, Kelly EJ, Rettie AE. Ocular cytochrome P450s and transporters: roles in disease and endobiotic and xenobiotic disposition. *Drug Metab Rev*. 2014;46:247–260.

72. Toselli F, Dodd PR, Gillam EMJ. Emerging roles for brain drug-metabolizing cytochrome P450 enzymes in neuropsychiatric conditions and responses to drugs. *Drug Metab Rev*. 2016; 48:379–404.

73. Wang K, Chen S, Xie W, Wan Y-JY. Retinoids induce cytochrome P450 3A4 through RXR/VDR-mediated Pathway. *Biochem Pharmacol*. 2008;75:2204–2213.

74. Hong S-P, Choi D-H, Choi J-S. Effects of resveratrol on the pharmacokinetics of diltiazem and its major metabolite, desacetyldiltiazem, in rats. *Cardiovasc Therap*. 2008;26: 269–275.

75. Szikra T, Barabas P, Bartoletti TM, et al. Calcium homeostasis and cone signaling are regulated by interactions between calcium stores and plasma membrane ion channels. *PLoS One*. 2009;4:e6723.

76. Guerra L, Cerbai E, Gessi S, Borea PA, Mugelli A. The effect of oxygen free radicals on calcium current and dihydropyridine binding sites in guinea-pig ventricular myocytes. *Br J Pharmacol*. 1996;118:1278–1284.

77. Kooragayala K, Gotoh N, Cogliati T, et al. Quantification of oxygen consumption in retina ex vivo demonstrates limited reserve capacity of photoreceptor mitochondria. *Invest Ophthalmol Vis Sci*. 2015;56:8428–8436.

78. Cingolani C, Rogers B, Lu L, Kachi S, Shen J, Campochiaro PA. Retinal degeneration from oxidative damage. *Free Radic Biol Med*. 2006;40:660–669.

79. Witola WH, Kim CY, Zhang X. Inherent oxidative stress in the Lewis Rat is associated with resistance to toxoplasmosis. *Infect Immun*. 2017;85:e00289–17.

80. Battelle BA, LaVail MM. Rhodopsin content and rod outer segment length in albino rat eyes: modification by dark adaptation. *Exp Eye Res*. 1978;26:487–497.

81. Sondereker KB, Onyak JR, Islam SW, Ross CL, Renna JM. Melanopsin ganglion cell outer retinal dendrites: morphologically distinct and asymmetrically distributed in the mouse retina. *J Comp Neurol*. 2017;525:3653–3665.

82. Ortin-Martinez A, Nadal-Nicolas FM, Jimenez-Lopez M, et al. Number and distribution of mouse retinal cone photoreceptors: differences between an albino (Swiss) and a pigmented (C57/BL6) strain. *PLoS One*. 2014;9: e102392.

83. Zhu Y, Natoli R, Valter K, Stone J. Differential gene expression in mouse retina related to regional differences in vulnerability to hyperoxia. *Mol Vis*. 2010;16:740–755.

84. Howell WL, Rapp LM, Williams TP. Distribution of melanosomes across the retinal pigment epithelium of a hooded rat: implications for light damage. *Invest Ophthalmol Vis Sci*. 1982;22:139–144.

85. Williams MA, Pinto LH, Gherson J. The retinal pigment epithelium of wild type (C57BL/6J +/+) and pearl mutant (C57BL/6J pe/pe) mice. *Invest Ophthalmol Vis Sci*. 1985;26:657–669.

86. Polosa A, Bessaklia H, Lachapelle P. Strain differences in light-induced retinopathy. *PLoS One*. 2016;11:e0158082.

87. Corbo JC, Myers CA, Lawrence KA, Jadhav AP, Cepko CL. A typology of photoreceptor gene expression patterns in the mouse. *Proc Natl Acad Sci U S A*. 2007;104:12069–12074.

88. Fox DA, Rubinstein SD. Age-related changes in retinal sensitivity, rhodopsin content and rod outer segment length in hooded rats following low-level lead exposure during development. *Exp Eye Res*. 1989;48:237–249.

89. Rapp LM, Fisher PL, Dhindsa HS. Reduced rate of rod outer segment disk synthesis in photoreceptor cells recovering from UVA light damage. *Invest Ophthalmol Vis Sci*. 1994;35:3540–3548.

90. Mao H, Seo SJ, Biswal MR, et al. Mitochondrial oxidative stress in the retinal pigment epithelium leads to localized retinal degeneration. *Invest Ophthalmol Vis Sci*. 2014;55:4613–4627.

91. Rapp LM, Williams TP. The role of ocular pigmentation in protecting against retinal light damage. *Vision Res*. 1980;20:1127–1131.

92. Yoshizawa K, Nambu H, Yang J, et al. Mechanisms of photoreceptor cell apoptosis induced by N-methyl-N-nitrosourea in Sprague-Dawley rats. *Lab Invest*. 1999;79:1359–1367.

93. LaVail MM, Matthes MT, Yasumura D, Steinberg RH. Variability in rate of cone degeneration in the retinal degeneration (rd/rd) mouse. *Exp Eye Res*. 1997;65:45–50.

94. Maeda A, Maeda T, Golczak M, Palczewski K. Retinopathy in mice induced by disrupted all-trans-retinal clearance. *J Biol Chem*. 2008;283:26684–26693.

95. Smit-McBride Z, Oltjen SL, Lavail MM, Hjelmeland LM. A strong genetic determinant of hyperoxia-related retinal degeneration on mouse chromosome 6. *Invest Ophthalmol Vis Sci*. 2007;48:405–411.

96. Liang L, Katagiri Y, Franco LM, et al. Long-term cellular and regional specificity of the photoreceptor toxin, iodoacetic acid (IAA), in the rabbit retina. *Vis Neurosci*. 2008;25:167–177.

97. Polosa A, Liu W, Lachapelle P. Retinotopic distribution of structural and functional damages following bright light exposure of juvenile rats. *PLoS One*. 2016;11:e0146979.

98. Stone J, Maslim J, Valter-Kocsi K, et al. Mechanisms of photoreceptor death and survival in mammalian retina. *Prog Retin Eye Res*. 1999;18:689–735.

99. Organisciak DT, Vaughan DK. Retinal light damage: mechanisms and protection. *Prog Retin Eye Res*. 2010;29:113–134.

100. Tushev G, Schuman EM. Rethinking functional segregation: gradients of gene expression in area CA1. *Neuron*. 2016;89:242–243.

101. Velez G, Machlab DA, Tang PH, et al. Proteomic analysis of the human retina reveals region-specific susceptibilities to metabolic- and oxidative stress-related diseases. *PLoS One*. 2018;13:e0193250.

102. Patel AK, Davis A, Rodriguez ME, Agron S, Hackam AS. Protective effects of a grape-supplemented diet in a mouse model of retinal degeneration. *Nutrition*. 2016;32:384–390.

103. Lederman M, Hagbi-Levi S, Grunin M, et al. Degeneration modulates retinal response to transient exogenous oxidative injury. *PLoS One*. 2014;9:e87751.

104. Chen H, Liu B, Lukas TJ, Suyeoka G, Wu G, Neufeld AH. Changes in iron regulatory proteins in the aged rodent neural retina. *Neurobiol Aging*. 2009;30:1865–1876.

105. Muralidharan P, Cserne Szappanos H, Ingley E, Hool L. Evidence for redox sensing by a human cardiac calcium channel. *Sci Rep*. 2016;6:19067.

106. Ko EA, Wan J, Yamamura A, et al. Functional characterization of voltage-dependent Ca2+ channels in mouse pulmonary arterial smooth muscle cells: divergent effect of ROS. *Am J Physiol Cell Physiol*. 2013;304:C1042–C1052.

107. Chaplin NL, Nieves-Cintron M, Fresquez AM, Navedo MF, Amberg GC. Arterial smooth muscle mitochondria amplify hydrogen peroxide microdomains functionally coupled to L-type calcium channels. *Circ Res*. 2015;117:1013–1023.

108. Yang L, Xu J, Minobe E, et al. Mechanisms underlying the modulation of L-type Ca2+ channel by hydrogen peroxide in guinea pig ventricular myocytes. *J Physiol Sci*. 2013;63:419–426.

109. León OS, Menéndez S, Merino N, et al. Ozone oxidative preconditioning: a protection against cellular damage by free radicals. *Mediators Inflamm*. 1998;7:289–294.

110. Chen J, Wang Q, Zhang H, et al. In vivo quantification of T1, T2, and apparent diffusion coefficient in the mouse retina at 11.74T. *Magn Reson Med*. 2008;59:731–738.

111. Berkowitz BA, Schmidt T, Podolsky RH, Roberts R. Melanopsin phototransduction contributes to light-evoked choroidal expansion and rod L-type calcium channel function in vivo. *Invest Ophthalmol Vis Sci*. 2016;57:5314–5319.

112. Ferguson LR, Dominguez JM II, Balaiya S, Grover S, Chalam KV. Retinal thickness normative data in wild-type mice using customized miniature SD-OCT. *PLoS One*. 2013;8:e67265.